rales Arnao, *Science* **226**, 50 (1984); L. G. Thompson, in *Climate Since A.D. 1500*, R. S. Bradley and P. D. Jones, Eds. (Routledge, London, 1992), p. 517–548.
5. D. H. Sandweiss, J. B. Richardson III, E. J. Reitz, H. B. Rollins, K. A. Maasch, *Science* **273**, 1531 (1996); *ibid.* **276**, 966 (1997).
6. W. H. Quinn and V. T. Neall, *in Climate Since A.D. 1500*, R. S. Bradley and P. D. Jones, Eds. (Routledge, London, 1992), pp. 623–648.
7. E. Cucalon, *J. Geophys. Res.* **92**, 14309 (1987).
8. J. D. Horel and A. G. Cornejo-Garrido, *Mon. Weather Rev.* **114**, 2091 (1986).
9. R. A. Goldberg and G. Tisnado, *J. Geophys. Res.* **92**, 14225 (1987).
10. G. S. Philander, *J. Atmos. Sci.* **42**, 2652 (1985).
11. We photographed cores digitally and processed these images with the National Institutes of Health program IMAGE. This program assigns a value between 0 (white) and 256 (black) to each pixel. Because each pixel represents ~0.3 mm of core and because gray scale is a good proxy for C content, the gray-scale record represents a proxy for the oscillation between inorganic, storm-induced clastic sedimentation and organic-rich background sedimentation with subannual resolution.
12. D. T. Rodbell, *Geol. Soc. Am. Bull.* **105**, 923 (1993).
13. The geochemistry of the organic matter indicates that most of the C supplied to the lake was derived from terrestrial sources during the deposition of light and dark laminae, as there is little difference between the organic matter contained in the two types of laminae. All the free and bound aliphatic biomarkers in both the light and dark laminae are dominated by *n*-alkanes ranging in C chain length from C_{21} to C_{35}. The chain length and a pronounced odd-over-even dominance suggest a terrestrial plant source, and the suite of biomarkers present is almost exclusively from a terrestrial plant source. These results are corroborated by similar C/N ratios and $\partial^{13}C$ values for both light and dark laminae.
14. Gray scale is a proxy indicator of C content ($Y = 10^{-14}X^{6.628}$, where Y is weight % of C and X is gray scale; $n = 32$ samples), and C content is a proxy for sediment bulk density ($Y = 0.282X^{-0.338}$, where Y is bulk density and X is weight % of C; $n = 447$ samples). Correlation coefficients for these equations are 0.89 and 0.82, respectively, and both exceed critical values at the 99.9% confidence level. From these equations, the mass of C represented by each pixel in the digital record can be estimated, and the total mass of accumulated C between dated intervals can be determined. From the total mass of C, the average rate of C deposition can be calculated, and time can then be allocated between AMS ^{14}C-dated intervals according to the gray-scale value, so that the lighter the color of sediment, the less time it represents (and vice versa).
15. The El Niño signal that is recorded in Laguna Pallcacocha may be complicated by other factors. Delta progradation may influence the delivery of clastic sediment to the deep basin, and we expect that this would cause a progressive increase in the grain size and thickness of the clastic layers; however, we have noted no such trends. Seismic activity may be responsible for clastic events, but it is unlikely that this would have a major effect on the periodicity of sedimentation within the 2- to 8.5-year ENSO band. Because most precipitation that falls in the tropical Andes is derived from the tropical easterlies, it is possible that the North Atlantic Oscillation is a compounding influence on interannual sediment delivery to the lake [Y. Kushnir, *J. Clim.* **7**, 141 (1994)].
16. The time series for each drive were interpolated at a 0.75-year interval (the minimum sample spacing). The trend and low-frequency variance were removed with a triangular-shaped filter with a 1/2 pass band frequency of 1/150 year. With 100 lags ($M = n/8$, where M is the number of lags), we calculated the variance spectrum as the Fourier transform of the autocovariance function, using the Blackman-Tukey method [G. M. Jenkins and D. G. Watts, *Spectral Analysis and Its Applications* (Holden-Day, Oakland, CA, 1968)] in the ARAND package from Brown University (Providence, RI). Confidence levels (80%) are based on the inverse chi-square distribution.
17. R. Vautard, P. Yiou, M. Ghil, *Physica D* **58**, 95 (1992).
18. D. J. Thompson, *Philos. Trans. R. Soc. London Ser. A* **330**, 601 (1990).
19. D. B. Enfield and L. Cid, *J. Clim.* **4**, 1137 (1991); K. E. Trenberth, *Bull. Am. Meteorol. Soc.* **78**, 2771 (1997); M. J. McPhaden *et al.*, *J. Geophys. Res.* **103**, 14169 (1998).
20. M. K. Gagan *et al.*, *Science* **279**, 1014 (1998).
21. On the basis of flood deposits intercalated with clay-enriched aridic soils along the hyperarid north coast of Perú, an alternative interpretation has been proposed, which asserts that the presence of TAMAs is a result of coastal geomorphology and sea-level rise rather than climate [T. J. DeVries, L. Ortlieb, A. Diaz, L. Wells, Cl. Hillaire-Marcel, *Science* **276**, 965 (1997); L. E. Wells and J. S. Noller, *ibid.*, p. 966] and that the ENSO persisted through at least the past 40,000 years (*3*). Our record clearly shows that storm-generated clastic depositional events occurred during the Late Glacial and early Holocene with periodicities of ≥15 years, but not in the 2- to 8.5-year ENSO band. The interpretation of the TAMA (*5*) is also problematic because it implies a quasi-permanent El Niño state, which is neither evident in our record as a prolonged period of clastic sedimentation, nor in other proxy records from the region (*3*). We suggest that whereas El Niños may have been less frequent, the eastern Pacific was marked by less intense upwelling and zonal circulation and was capable of producing infrequent and localized coastal flooding but was insufficient to generate high-frequency convective-driven precipitation to 4000 masl.
22. M. S. McGlone, A. P. Kershaw, V. Markgraf, in *El Niño: Historical and Paleoclimatic Aspects of the Southern Oscillation*, H. F. Diaz and V. Markgraf, Eds. (Cambridge Univ. Press, Cambridge, 1992), pp. 434–462.; J. Shulmeister and B. G. Lees, *Holocene* **5**, 10 (1995).
23. L. G. Thompson *et al.*, *Science* **269**, 46 (1995).
24. D.-Z. Sun, in *El Niño and the Southern Oscillation: Multiscale Variability, Global and Regional Impacts*, H. F. Diaz and V. Markgraf, Eds. (Cambridge Univ. Press, Cambridge, in press).
25. G. L. Pickard and W. J. Emery, *Descriptive Physical Oceanography* (Pergamon, Oxford, 1982).
26. A. Berger, *Quat. Res.* **9**, 139 (1978).
27. M. Stuiver and P. J. Reimer, *Radiocarbon* **35**, 215 (1993).
28. We thank R. Fleischer, P. Gremillion, and anonymous reviewers for improving the manuscript and C. Oballe and K. Reed for their help in retrieving the sediment core. Supported by NSF grants EAR9418886 (D.T.R.) and EAR9422424 (G.O.S.) and by the Union College Internal Education Foundation (J.H.N.) and Faculty Research Fund (D.T.R.).

20 October 1998; accepted 11 December 1998

Nanophase-Separated Polymer Films as High-Performance Antireflection Coatings

Stefan Walheim, Erik Schäffer, Jürgen Mlynek, Ullrich Steiner*

Optical surfaces coated with a thin layer to improve light transmission are ubiquitous in everyday optical applications as well as in industrial and scientific instruments. Discovered first in 1817 by Fraunhofer, the coating of lenses became standard practice in the 1930s. In spite of intensive research, broad-band antireflection coatings are still limited by the lack of materials with low refractive indices. A method based on the phase separation of a macromolecular liquid to generate nanoporous polymer films is demonstrated that creates surfaces with high optical transmission.

Light reflection off glass surfaces is undesirable, disturbing, and limits the performance of devices for which maximum light transmission is required (such as solar cells). Antireflection (AR) coatings reduce the intensity of reflection and increase the quality of optical lens systems. The basic principle of optical coatings can easily be understood as follows (*1*). The reflected light from the air-film and film-substrate interfaces must interfere destructively to maximize the light transmission into the transparent substrate (Fig. 1A). Two conditions must be met: (i) The light amplitudes reflected at both interfaces must be equal; that is, $n_0/n_f = n_f/n_s$ or $n_f = \sqrt{n_0 n_s}$, with n_0, n_f, and n_s being the refractive indices of air, film, and substrate respectively; and (ii) the optical path length must be chosen for the reflected wave to interfere destructively; that is, the film thickness must be 1/4 of a reference wavelength in the optical medium. Although condition (ii) can be easily met, condition (i) poses a problem: Refractive indices for glass and transparent plastic substrates are ≈1.5, therefore requiring that $n_f \approx 1.22$. Because the lowest refractive indices for dielectrics are on the order of 1.35, single-layer AR coatings cannot attain this value. For broad-band AR coatings, a sequence of layers is needed that have refractive indices varying stepwise from n_0 to n_s. In this case, $n_f < 1.22$ is desirable.

Instead of a homogeneous layer, a nanoporous film can be used. If the pore size is much smaller than the visible wavelengths, the effective n of the nanoporous medium is given by an average over the film. The challenge is to maximize the volume ratio of pores in order to achieve the refractive indi-

Fakultät für Physik, Universität Konstanz, D-78457 Konstanz, Germany. www.uni-konstanz.de/FuF/Physik/Mlynek/Steiner/

*To whom correspondence should be addressed. E-mail: ulli.steiner@uni-konstanz.de

ces needed for a broad-band AR coating. The idea to use nanoporous films as AR coatings is not new. Indeed, the etching procedure described by Fraunhofer in 1819 to tarnish glass is based on this principle (*1, 2*). More modern approaches include sol-gel derived coatings (*3*) and patterned surfaces with submicrometer gratings (*4, 5*). High-performance coatings, tailored to the varying requirements of different applications, require films whose thickness and refractive indices can be fine-tuned with great precision. In particular, AR layers with extremely low refractive indices ($n_f \leq 1.1$) are needed for high-performance multilayer AR coatings.

We present here a general procedure for creating nanoporous polymer films for use as AR coatings. Our technique is based on the demixing of a binary polymer blend during spin coating (*6, 7*) (Fig. 1B). As prepared, the polymer film typically exhibits a lateral phase morphology that strongly depends on a number of preparation parameters (*6*). The thin films on transparent substrates appear featureless and transparent. Because most polymers have similar refractive indices to glass ($n \approx 1.5$), there is no visible difference in the reflected light between coated and uncoated surfaces. To create a porous film, one of the two polymers is removed by exposing the film to a selective solvent that dissolves one of the two components (Fig. 1C), which changes the optical appearance of the film. Two cases can be distinguished: (i) For pore sizes comparable to or greater than the wavelength of light, the film appears opaque because the light scatters off the porous structure; and (ii) if all length scales of the lateral phase morphology lie much below all optical wavelengths, the nanoporous film remains transparent. A remarkable difference is detected when the reflection of a film-covered surface is examined: The nanoporous layer reduces the intensity of reflected light (*8*).

We demonstrated the general applicability of this procedure using standard polymers and solvents (*9*). Polystyrene (PS) and polymethylmethacylate (PMMA) were dissolved in tetrahydrofuran (THF) and spin-cast onto both sides of a microscope slide (*10*). After exposing the glass slide to cyclohexane, which selectively dissolves PS, we obtained porous films. Apart from a visual examination of the slide, which gives a good estimate of its optical quality, atomic force microscopy (AFM), ellipsometry, and transmission measurements (*11*) were used to characterize the film quantitatively.

In Fig. 2, typical AFM images of porous films are shown (*12*). For the opaque film in Fig. 2A, the micrometer-sized pores can be readily imaged. The AFM investigation of a nanoporous film in Fig. 2B verifies the absence of lateral structures larger than 100 nm and reveals a rough surface rather than individual pores. Because AFM images are always a convolution of the surface topography with the tip shape, the radius of curvature of the tip (20 nm) limits the resolution, which is most visibly seen in Fig. 2B.

The optical transmission spectra of a glass slide covered on both sides with a 106-nm-thick nanoporous PMMA film (Fig. 3A, circles) is well approximated by a refractive index of 1.255 (Fig. 3A, line). For comparison, an uncoated glass slide (Fig. 3A, squares) and a conventional AR coating, consisting of 99-nm-thick magnesium fluoride (MgF_2) layers (n_f = 1.381), are shown. The polymer AR coating increases the optical transmission through the glass slide (averaged from 400 to 680 nm) from 91 to 99.3%, as compared to the industrial standard, MgF_2, with an increase to only 97%. In particular, for one reference wavelength λ_{max} = 534 nm, a transmission near 100% (>99.95%) is achieved.

A major advantage of our approach is its versatility. For AR coatings, the ability to fine-tune n_f and layer thickness are of high priority. In the case of nanoporous polymer films, both can easily be achieved. Because the wavelength maximum of the transmission spectrum (λ_{max}) scales linearly with the layer thickness ℓ ($\lambda_{max} = 4n\ell$), a simple variation of the layer thickness (by varying the spin-coating speed) adjusts the location of λ_{max} (Fig. 3B). More important, however, is the fine-tuning of n_f. Because the effective refractive index is a function of the pore volume ratio in the film, a variation of the volume fraction of PS in the film varies the refractive index of the nanoporous film (Fig. 4, open squares). The empirical dependence of the refractive index on the polymer mixing ratio allows a precise adjustment of the refractive index.

Multilayers further reduce the reflected light but require layers of refractive index below 1.2. To create layers of extremely high porosity, more polymer must be removed from the film. To achieve this, some of the PMMA in the solution is replaced by PMMA of a lower molecular weight (M_w) (*13*). As before, the coated surface is washed in cyclohexane to remove the PS phase, which produces a film with n_f = 1.2. The nanoporous film is then exposed to ethanol, which does not dissolve high-M_w PMMA but

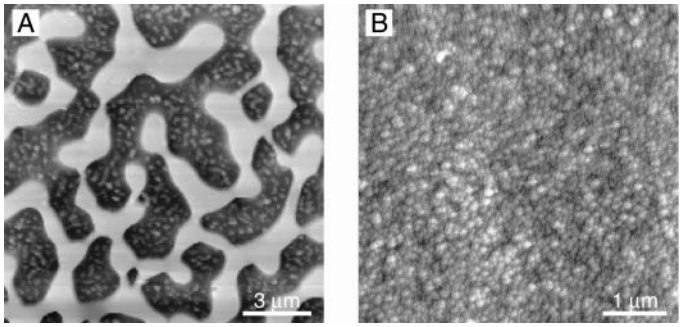

Fig. 2. Atomic force microscope images of two porous PMMA films ≈110 nm thick. After spin-casting of a PS-PMMA-THF mixture onto silicon oxide surfaces, the PS phase was removed by washing the sample in cyclohexane (*12*). (**A**) Films prepared from higher M_w PS and PMMA show average structure sizes of ≈1 μm. (**B**) If low M_w PS and PMMA are used, the lateral structure size is reduced to ≈100 nm. Although the film in (A) appears opaque, the nanoporous film in (B) is transparent with a low effective refractive index.

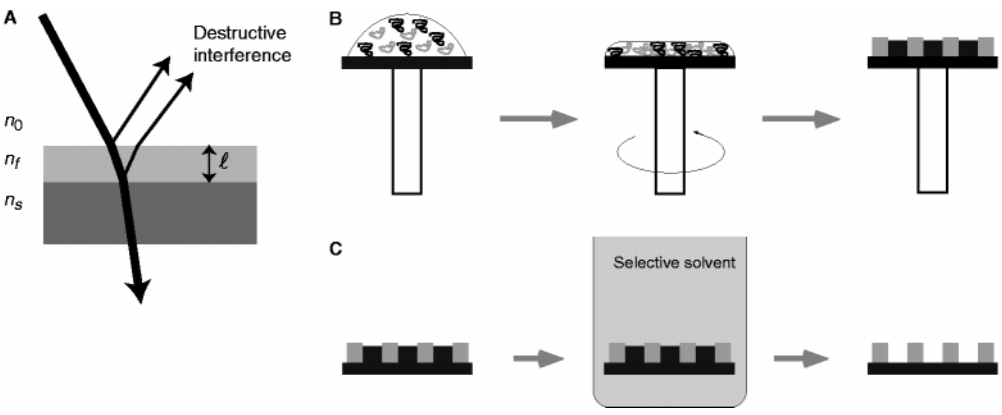

Fig. 1. (**A**) Reflection of light from both interfaces of an AR layer. For a given wavelength and incidence angle, light transmission is maximized when the two reflected beams interfere destructively. (**B**) Preparation of a binary polymer film. Initially, both polymers (black and gray) and the solvent form one phase. During spin-coating, phase separation sets in, and after evaporation of the solvent a lateral phase morphology is obtained. (**C**) The film is exposed to a solvent that is selective for one of the polymers, producing a porous film.

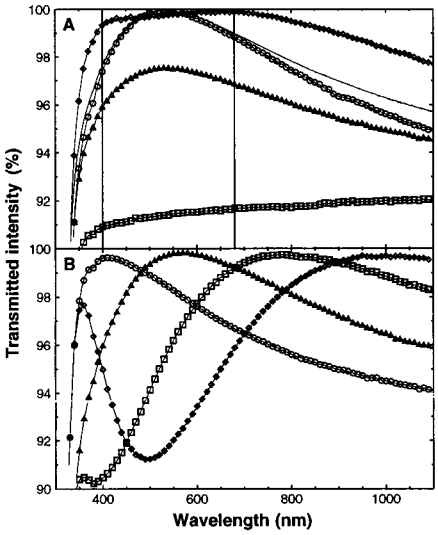

Fig. 3. Light transmission versus wavelength of microscope glass slides that were covered on both sides with AR layers. (**A**) The nanoporous coating from Fig. 2B (circles) exhibits a light transmission of >99.95% at $\lambda = 534$ nm. The solid line is a calculated curve for an AR layer with $n_f = 1.255$ and thickness $\ell = 106$ nm. In comparison, a 99-nm-thick MgF_2 coating with $n_f = 1.381$ (triangles) and an uncoated glass slide (squares) are shown. A broad-band AR coating is obtained when the MgF_2 layers are coated with a nanoporous polymer film with $n_f = 1.14$ and $\ell = 115$ nm (diamonds) (*14*). The slide with this double-layer coating exhibits a transmission of >99.7% averaged over the visible wavelengths (vertical lines). (**B**) Slides were covered on both sides with nanoporous PMMA films ($n_f = 1.285$) of varying thickness as follows: 80 nm (circles), 110 nm (triangles), 150 nm (squares), and 195 nm (diamonds). For the thickest film (diamonds), a second-order maximum appears that is due to the destructive interference of the two reflected beams phase-shifted by $3\lambda/2$.

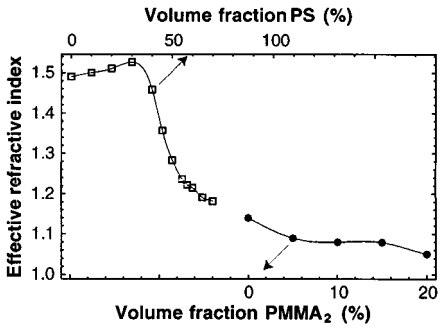

Fig. 4. Variation of the refractive index as a function of polymer composition. The open squares correspond to PS-PMMA mixtures with PS volume fractions varying from 0 to 70%. The film thickness was ~150 nm. After removal of the PS (by washing for 30 s in cyclohexane), refractive indices down to $n_f = 1.2$ were obtained. To further lower the refractive index, ternary mixtures of PS, $PMMA_1$, and $PMMA_2$ were used (*13*). The removal of PS and $PMMA_2$ leads to a further reduction of the refractive index but also reduces the film thickness to ≈70 nm. Refractive indices as low as $n_f = 1.05$ were obtained (solid circles).

does dissolve low-M_w PMMA to some extent. The solid circles in Fig. 4 show the refractive index of the AR layer as a function of the low-M_w PMMA volume fraction ($PMMA_2$) corresponding to a reduction of n_f from 1.2 to 1.05.

These results allow one to proceed toward multilayer systems with enhanced transmission over the entire visible spectrum. Unfortunately, the low-refractive-index films in Fig. 4 are too thin to be suitable as AR coatings. An increase in film thickness leads to larger PS-PMMA domain sizes (*6*) and therefore to more scattered light. This effect can be suppressed by adding small amounts of amphiphilic molecules (PS-PMMA diblock copolymer) to the solution (*14*). A nanoporous film with $n_f = 1.14$ was prepared from a PS-PMMA-diblock mixture on both sides of a glass slide. Before the polymer deposition, the glass slide was covered on both sides with a 99-nm-thick MgF_2 layer. After exposure of the sample to cyclohexane, a visual inspection of this bilayer system showed practically no discernible reflection of light. The transmission spectrum in Fig. 3A (diamonds) shows a broad-band AR coating of outstanding quality with a transmission of 99.7% averaged over the entire visible spectrum. This result suggests a strategy in which a double layer could be entirely made of polymers: A homogeneous polymer film with $n_f = 1.36$ (that is, an amorphous fluoropolymer) is first deposited on the substrate and is then covered by a nanoporous polymer layer. Because fluoropolymers are not soluble in the solvents we used, the AR coating can be prepared in a repeated spin-coating process.

Our work makes use of a simple but fundamental principle—the demixing of mutually incompatible macromolecular liquids and the subsequent removal of one or more phases with selective solvents. For very short demixing times, the polymer domain sizes are smaller than the wavelength of light, and the porous films are effective AR coatings. The improvement in the light transmission of a few percent per air-glass interface may seem small, but its cumulative effect in a lens system with more than 20 glass surfaces is considerable. Although the general strategy of using porous films as AR coatings is well established, optimized two- and three-layer coatings ($n \approx 1.12$ for two layers and $n \approx 1.06$ for three layers) are now possible as very low refractive indices have been achieved. Polymer-based AR layers can easily be fine-tuned to produce a wide range of refractive indices. Their manufacture is inexpensive, reproducible, and takes just a few minutes without the need for specialized equipment. By using appropriate combinations of polymers and solvents, it will be possible to create multilayers consisting entirely of polymers in repeated spin-coating runs.

Although the AR coatings made from model polymers (PMMA) are not wear-resistant, this is not a major limitation of our approach because the underlying principle works for a large number of polymers, and materials with improved mechanical characteristics can be chosen (such as fluoropolymers). Alternatively, the application of our approach to organic-inorganic hybrid materials allows one to replicate the nanoporous polymer films (*15*) into mineralized AR coatings with extremely low refractive indices.

References and Notes

1. H. A. Macleod, *Thin-Film Optical Filters* (Hilger, Bristol, UK, 1986).
2. M. J. Minot, *J. Opt. Soc. Am.* **66**, 515 (1976).
3. D. R. Uhlmann, T. Suratwala, K. Davidson, J. M. Boulton, G. Teowee, *J. Non-Cryst. Solids* **218**, 113 (1997).
4. C. Heine and R. H. Morf, *Appl. Opt.* **34**, 2476 (1995).
5. S. J. Wilson and M. C. Hutley, *Opt. Acta* **29**, 993 (1982).
6. S. Walheim, M. Böltau, J. Mlynek, G. Krausch, U. Steiner, *Macromolecules* **30**, 4995 (1997).
7. M. Böltau, S. Walheim, J. Mlynek, G. Krausch, U. Steiner, *Nature* **391**, 877 (1998).
8. A patent application for this method was filed with the German Patent Office on 26 June 1998 under number 198 29 172.8.
9. Nanoporous films based on a PS-polyvinylchloride mixture show practically identical results (S. Walheim and U. Steiner, unpublished material).
10. All polymers were purchased from Polymer Standards Service in Mainz and were used as obtained. Polymer polydispersities were 1.1 and lower. As solvents, analytic grade THF [stabilized with 2.6-di-*tert*-butyl-4-methylphenol (250 mg/liter)], cyclohexane, and ethanol were used. Standard microscope glass slides 1 mm thick were used as substrates.
11. Atomic force microscopy measurements were carried out on a self-built AFM. Layer thicknesses and refractive indices were measured with a single-wavelength ($\lambda = 632.8$ nm) ellipsometer (Riss Ellipsometerbau, model EL X-1). For the ellipsometry measurements, polished silicon wafers were used as substrates. Light transmission spectra were measured with a Perkin Elmers Lambda 40 spectrometer at vertical incidence with an open reference beam.
12. The film in Fig. 2A was cast from a THF solution (3% polymer by weight) of PS ($M_w = 94.4$ kg/mol) and PMMA ($M_w = 100$ kg/mol) (50:50% w/w). In Fig. 2B, a mixture of PS ($M_w = 10.3$ kg/mol) and PMMA ($M_w = 10.6$ kg/mol) (70:30% w/w) in THF (2% polymer by weight) was used. In both cases, the PS phase was removed by exposing the sample for 1 min to cyclohexane.
13. A ternary mixture of PS ($M_w = 10.3$ kg/mol, 60% by weight), $PMMA_1$ ($M_w = 10.6$ kg/mol), and $PMMA_2$ ($M_w = 1.96$ kg/mol) in THF (2% polymer by weight) was used. The as-cast films were exposed for 30 s to cyclohexane to remove the PS phase and subsequently for 10 s to ethanol, which partially dissolves $PMMA_2$.
14. A mixture of PS ($M_w = 1.92$ kg/mol), PMMA ($M_w = 1.96$ kg/mol), and a PS-PMMA diblock [$M_w = 54$(PS)-54(PMMA) kg/mol] (57.5:37.5:5% w/w/w) in THF (2% polymer by weight) was used. The sample was exposed for 30 s to cyclohexane to remove the PS phase.
15. M. Templin *et al.*, *Science* **278**, 1795 (1997).
16. Supported by the Deutsche Forschungsgesellschaft (DFG) (grant SFB 513, B2). U.S. acknowledges financial support by a research fellowship (Habilitations-Stipendum) of the DFG. We thank S. Eggert and T. P. Russell for useful discussions, H.-J. Apell for the use of his spectrometer, R. Adams for his help with the manuscript, and R. Müller for his help with the experiments.

2 October 1998; accepted 9 December 1998

Nanophase-Separated Polymer Films as High-Performance Antireflection Coatings

Stefan Walheim, Erik Schäffer, Jürgen Mlynek and Ullrich Steiner

Science **283** (5401), 520-522.
DOI: 10.1126/science.283.5401.520